Projection quality improvement with embedded illumination modulator in projector system

Chu-Ming Cheng and Jyh-Long Chern*

Department of Photonics, Institute of Electro-Optical Engineering, Microelectronics and Information System Research Center, National Chiao Tung University, Hsinchu, Taiwan, China
chuming.eo92g@nctu.edu.tw

*Corresponding author: jlchern@faculty.nctu.edu.tw

Received 10 February 2010; revised 18 April 2010; accepted 20 April 2010;
posted 26 April 2010 (Doc. ID 123983); published 31 May 2010

We demonstrate an approach for improving the image quality for a projector system with a shape-programmable pupil, which could be generated by an illumination modular in which a digital micromirror device is embedded. Essentially, the shaped pupil from the illumination modulator is developed with a dynamically programmable approach to provide aberration compensation for the projection system. By analyzing the optical transfer function, the resolution limit of an imaging system with specific defocus, spherical aberration and coma are shown to be improved significantly with a binary-shaped pupil. It is found that the improvement of the projection quality could be characterized by the scale ratio of $K = c/D$, defined as the ratio between the resolution scale of structured light, c, and the size scale of the aperture stop, D. When K is equal to 0.05, the low-frequency components of the image could be improved, while if K is equal to 0.3, the imaging quality of the image at high-frequency components can be enhanced in a defocused system. Furthermore, as K ranges from 0.05 to 0.3, the imaging performance of the optical contrast could be enhanced in a projector system with large coefficients of defocused, spherical aberration and coma.

OCIS codes: 110.2960, 110.2945, 110.4850, 220.1000, 230.4685.

1. Introduction

Projection display technology is widely applied to the large-screen display for autostereoscopic 3D projectors, business projectors, and rear-projection TVs, mostly based on three different light valves, such as the transmissive liquid crystal device (LCD), digital micromirror device (DMD), and liquid crystal on silicon (LCoS) [1]. In the field of optics, the technologies involved are being applied to very compact systems with high imaging performance specifications. Consequently, designs for higher resolution image, larger optical collection efficiency, and smaller volume optical systems are required. It is known that enhancing the quality of an image can be achieved and determined not only by the pupil function but also by its amplitude transmittance [2]. Nonuniform amplitude transmission filters can be employed to vary the response of an optical imaging system, for instance, to increase the focal depth and to decrease the influence of spherical aberration. Earlier investigations and experiments were carried out on annular apodizers [3,4] and nonuniform-shaped apertures [5] in imaging systems. However, none of those are programmable for the amplitude transmission at the aperture stop in a projection system. From the point of view of potential applications, as well as from a purely academic perspective, it is worthwhile to explore the possibility of realizing a programmable shaped pupil for projector systems.

It should be noted that in the literature of coherent illumination, amplitude-transmitting filters for apodizing and hyperresolving have been demonstrated to provide excellent axial resolution for the in-focus field by using a spatial light modulator, as shown in Refs. [6,7], where a programmable liquid-crystal spatial light modulator was used to be

0003-6935/10/163127-13$15.00/0

operated in transmission-only mode for a coherent imaging system with a laser light source, polarizers and quarter-wavelength plates. An incoherent imaging and spatial filtering system using a spatially discrete illumination characterized by a linear-in-intensity relationship between object and image distributions was demonstrated by Gracht and Rhodes [8]. In viewing the importance and potential value to practical application, a programmable apodizer using a digital micromirror device was recently proposed and has been numerically investigated to extend the depth of focus in an incoherent imaging system with defocus, as shown in Ref. [9].

In this paper, we will extend our early work of the imaging system shown in Ref. [9] to a projector system and numerically demonstrate the improvement of image quality in such a projector system with a shape-programmable shaped pupil, which is generated by a specific illumination modular with the DMD (Texas Instruments, Dallas, Texas) [10]. We will evaluate the imaging properties of the projection system with defocus, spherical aberration, and coma, where a specifically shaped pupil on the aperture stop is embedded, by calculating the optical transfer function (OTF) using the Hopkins method [11]. We also take the computer-simulated images of resolution patterns to explore the projection image performance. The remainder of this paper is organized as follows. In Section 2, the configuration of the proposed projector system, which consists of an illumination modulator and a projection module, is illustrated. In Section 3, we derive the pupil functions of the differently shaped pupil that are generated by the digital micromirror device. Then, in Section 4, we calculate the OTF in such a projector system. Furthermore, the corresponding OTFs are evaluated, and then we identify the projection performance for a system of perfect imaging (aberration-free) as well as the defocused, spherical, and coma aberrations in Section 5. Finally, conclusions are given in Section 6.

2. Configuration of Optical System

The schematic diagram of the projector system is illustrated in Fig. 1. The system consists of an illumination modulator and a projection module. The illumination modulator is formed by a uniform white light source (typically, for example, a white high-brightness light-emitting diode or high-pressure mercury lamp), a prism module and a DMD [10]. Obviously, the implementation is not limited by this kind of practical device. The projection module is a projection lens.

In the illumination modulator, by following the optical path of the illumination rays, as indicated by the dotted lines in Fig. 1, the rays starting from a uniform light source pass through lens 1 and a prism module. The size of the axial cone of energy from the light source is limited by the active area on the DMD. The DMD consists of hundreds of thousands of moving micromirrors that are made to rotate to either $+12°$ or $-12°$ positions depending on the binary state, i.e., on-state or off-state, of the underlying complementary metal oxide semiconductor synchronized dynamic random access memory cells below each micromirror [10]. The DMD array size is 1024×768, and the pixel micromirrors measure $\sim 13.7\ \mu$m square to form a matrix having a high fill factor of more than 90%. The prism system comprises two transparent prisms with an air gap between them. Total internal reflection (TIR) at the interface between the prism and the air gap is utilized to separate the rays by their angles. The TIR prism has been applied into the DMD-based projection display [12]. The prism system can guide the rays onto and away from the DMD simultaneously. The rays, indicated by the solid lines in Fig. 1 from the DMD, are imaged onto the aperture stop in the projection system by lens 2 and lens 3 when the configuration of the DMD is in the on state. When the configuration of the DMD is in the off state, the rays are steered away in the opposite direction, and the rays from the DMD are not imaged onto the aperture stop. In the projection system, the optical path of the imaging rays, as indicated by the dashed lines in Fig. 1, start from the light valve and pass through lens 3 and lens 4 and then are imaged onto the screen. The light valve utilized here is a transmissive LCD with the angular dependence of the transmittance, which could reduce the amplitude transmittance, especially on the peripheral area of the aperture stop. We assume that angular dependence of the transmissive LCD could be ignored for simplification because the incident angle of the illumination light onto the LCD panel is about $12° - 14.5°$, which is equivalent to the f numbers $2.0 - 2.4$ in a typical projector system, much smaller than the viewing angle of a typical LCD panel [13]. Obviously, implementation is not limited by this kind of device, for example, we could also use DMD and LCoS. The size of the axial cone from the light valve is limited by the f number of the projection lens module, the acceptable cone angle, the physical size of the light valve, and the f number of the illuminator modulator, according to the etendue theorem, which is an optical invariant of a light beam relative to the beam divergence

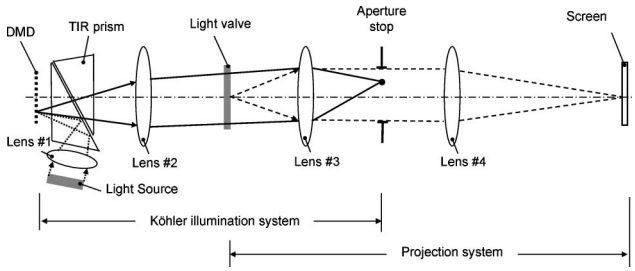

Fig. 1. Schematic diagram of the projector system with a Köhler illumination subsystem and a projection subsystem to illustrate the relationship between the aperture stop and the digital micromirror device. The dotted and solid lines indicate the optical path of the illumination rays in a Köhler illumination system. The dashed lines indicate the optical path of the imaging rays in a projection system.

and cross-sectional area for estimating maximum collection efficiency in a projection system [1].

By following the optical path of the illumination rays, as indicated by the solid lines in Fig. 1, the aperture stop in the projection system is designed to be a conjugate with the DMD plane by using lenses 2 and 3. For simplification in illustration, we assume that the pupil aberration is corrected and could be ignored for this Köhler illumination system. For the entire optical system, the DMD performs a spatial light modulation to rapidly and field-sequentially generate a specifically shaped pupil with either uniform or nonuniform illumination distribution on the aperture stop of the projection system.

3. Calculation of Pupil Functions

The pupil function of an optical system with defocused, spherical aberration and coma for a circular symmetrical aperture is given by [3]

$$f(x,y) = T'(x,y)\exp\{ik[\omega_{20}(x^2+y^2) + \omega_{40}(x^2+y^2)^2 + \omega_{31}(x^2+y^2)\times y]\} \quad x^2+y^2 \le 1$$
$$= 0 \quad x^2+y^2 > 1 \tag{1}$$

where ω_{20} is the wave aberration of the defocus coefficient, ω_{40} denotes the coefficient for spherical aberration, and ω_{31} denotes the coefficient for coma aberration. (x,y) are the normalized Cartesian coordinates, and $k = 2\pi/\lambda$, where λ is the wavelength of the ligcht. Function $T'(x,y)$ in Eq. (1) represents the binary amplitude distribution over the normalized pupil coordinate that is scaled and normalized to make the outer periphery the unit circle, $x^2+y^2 \le 1$. The binary amplitude transmittance $T'(x,y)$ is generated by the DMD, as shown in Fig. 2. We can derive the amplitude transmittance of the shaped aperture $T'(x,y)$ in an on-state configuration as follows:

$$T'(x,y) = E'(x,y) \otimes \sum_m \sum_n T(x,y)\delta\left(x - \frac{2mc}{D}\right)\delta\left(y - \frac{2nc}{D}\right), \tag{2}$$

$$0 \le |m|, |n| \le \mathrm{Int}\left[\frac{D/c - 1}{2}\right], \tag{3}$$

where $\otimes$ represents the convolution operation, $T(x,y) = 1 - (x^2+y^2)$ denotes the amplitude transmittance with a continuous profile at the aperture stop, which can extend the focal depth in the imaging system with a conventional annular apodizer [3], D is the corresponding diameter of the effective aperture stop, and c represents the width of each square individual aperture generated by DMD in the pupil plane, which is equal to an integer multiple of the value d, with d being the width of each square pixel in the DMD. Furthermore, $\delta[x - (2mc/D)]\delta[y - (2nc/D)]$ denotes the delta function, indicating the location of the individual aperture in the normalized coordinate on the aperture stop. $E'(x,y) = [H(x + c/D) - H(x - c/D)] \times [H(y + c/D) - H(y - c/D)]$ is the binary amplitude transmittance of the individual shaped aperture, which is then scaled and normalized into the pupil coordinate. $\mathrm{Int}[(D/c - 1)/2]$ is the interpart of $[(D/c - 1)/2]$. $H(x + c/D)$, $H(x - c/D)$, $H(y + c/D)$, and $H(y - c/D)$ are the step functions. It is evident that the total aperture function is formed by convolving the individual aperture function with an appropriate array of the delta function, each located at one of the coordinate origins $(x_m, y_n) = (2mc/D, 2nc/D)$, where $m, n = \ldots -2, -1, 0, 1, 2, \ldots$

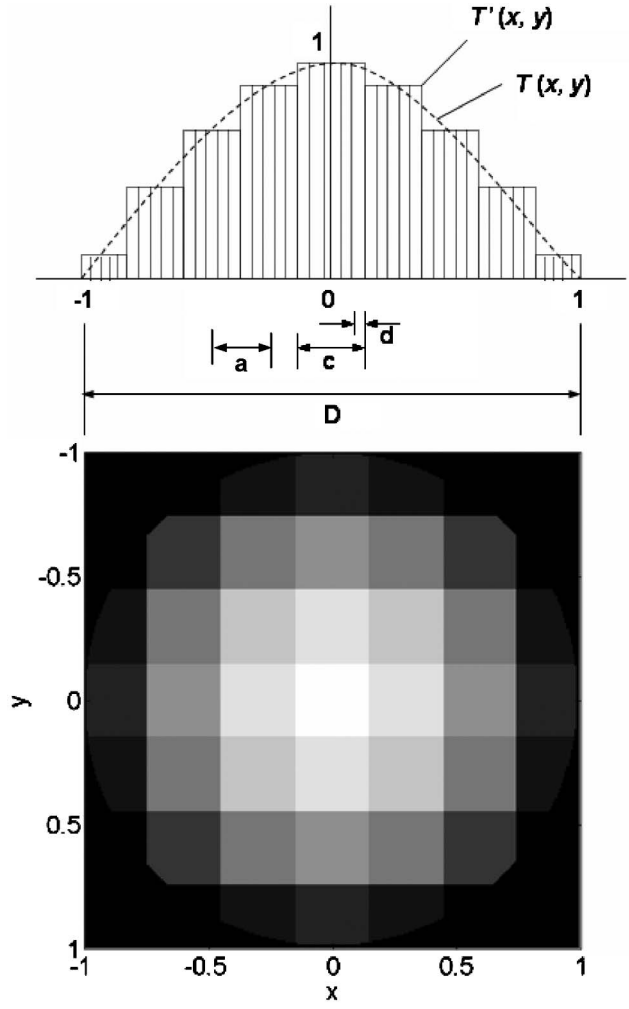

Fig. 2. Illustration of the binary amplitude transmittance $T'(x,y)$ for the normalized circular aperture, which is generated by the DMD. $T(x,y)$ represents a specifically shaped aperture for a conventional annular apodizer.

As will be shown, the quality of performance could be identified by a scale ratio, which is defined as

$$K \equiv (c/D). \tag{4}$$

The value of the scale ratio K determinates how many resolutions, how many gray levels, and how fast the DMD can dynamically generate the shaped

apertures within a specific exposure time. It is worthwhile to give an example for the quantity reference. If the DMD array is 1024×768 with a pixel size of 13.7 μm square, and the active area is 14.03 mm $\times$ 10.52 mm $= 147.60$ mm^2 [10], then the number of D is $\sim$10.52 mm (i.e., equal to the width of the active area of the DMD), provided that the effective aperture stop is located on the circular area centered at the actual DMD. In the case of $K = 0.05$, the width of each individual square aperture c is 0.53 mm and is equivalent to 38 square pixels with the same amplitude transmittance. There are 10 {i.e., $\mathrm{Int}[(D/c - 1)/2] + 1$} gray levels for a specifically shaped aperture, including the full bright mode and full dark mode. The current DMD-based system can offer 8 bits or 256 gray levels within a time period of 5.6 ms per primary color [10]. Thus, the DMD can rapidly generate one shaped aperture with 10 gray levels within the very short exposure time of 0.22 ms (i.e., $5.6 \times 10/256$) in the case of $K = 0.05$.

The computer program for evaluating Eqs. (2)–(4) is written with Mathematica software [14]. We assumed $D = 2$ for simplification and evaluated three different scale ratios, i.e., $K = 0$, $K = 0.05$, and $K = 0.3$. The binary amplitude transmittances of the shaped apertures $T'(x,y)$ are shown in Figs. 3(a)–3(d). The scale ratio $K = 0$ stands for the amplitude transmittance with a continuous profile. It is evident that the scale level of the binary amplitude transmission at the aperture stop increases with the reduction of scale ratio K, and the distribution of the binary amplitude transmission gets close to the continuous profile if the scale ratio K decreases.

In order to evaluate the relationship between the image performance and the size of the individual square aperture on the normalized pupil (i.e., fill factor or aperture ratio), we modified Eqs. (2) and (3) to the following equations:

$$T'(x,y) = E'(x,y) \otimes \sum_m \sum_n T(x,y)\delta\left(x - \frac{2ma}{D}\right)\delta\left(y - \frac{2na}{D}\right), \quad (5)$$

$$0 \le |m|, |n| \le \mathrm{Int}\left[\frac{D/a - 1}{2}\right] + 1, \quad (6)$$

where $\otimes$ represents the convolution operation. $T(x,y) = 1 - (x^2 + y^2)$ is the amplitude transmittance with a continuous profile at the aperture stop, D is the corresponding diameter of the effective aperture stop, c represents the width of each square individual aperture generated by DMD in the pupil plane. The parameter a represents the distance between each square individual aperture, as shown in Fig. 2. $\delta[x - (2ma/D)]\delta[y - (2na/D)]$ denotes the delta function, indicating the location of the individual aperture in the normalized coordinate on the aperture stop. $E'(x,y) = [H(x + c/D) - H(x - c/D)] \times [H(y + c/D) - H(y - c/D)]$ is the amplitude transmittance of the individual shaped aperture, which is then scaled and normalized into the pupil coordinate. $\mathrm{Int}[(D/a - 1)/2]$ is the interpart of $[(D/a - 1)/2]$ and $H(x + c/D)$, $H(x - c/D)$, $H(y + c/D)$, and $H(y - c/D)$ are the step functions. It is evident that the total aperture function is formed by convolving the individual aperture function with an appropriate array of the delta function, each located at one of the coordinate origins $(x_m, y_n) = (2ma/D, 2na/D)$, where $m, n = \ldots -2, -1, 0, 1, 2, \ldots$ We also take $D = 2$ and $a/D = 0.3$ in Eqs. (5) and (6). The fill factor represents the ratio of c and a. The amplitude transmittances $T'(x,y)$ with the fill factors 90% and 80% were computed as shown in Figs. 3(e) and 3(f). There are nine apertures (3×3 array) within the pupil. The results show that the individual aperture size on the normalized pupil is shrunk when the fill factor decreased. That is equivalent to the term $E'(x,y)$ varied with c in Eq. (5).

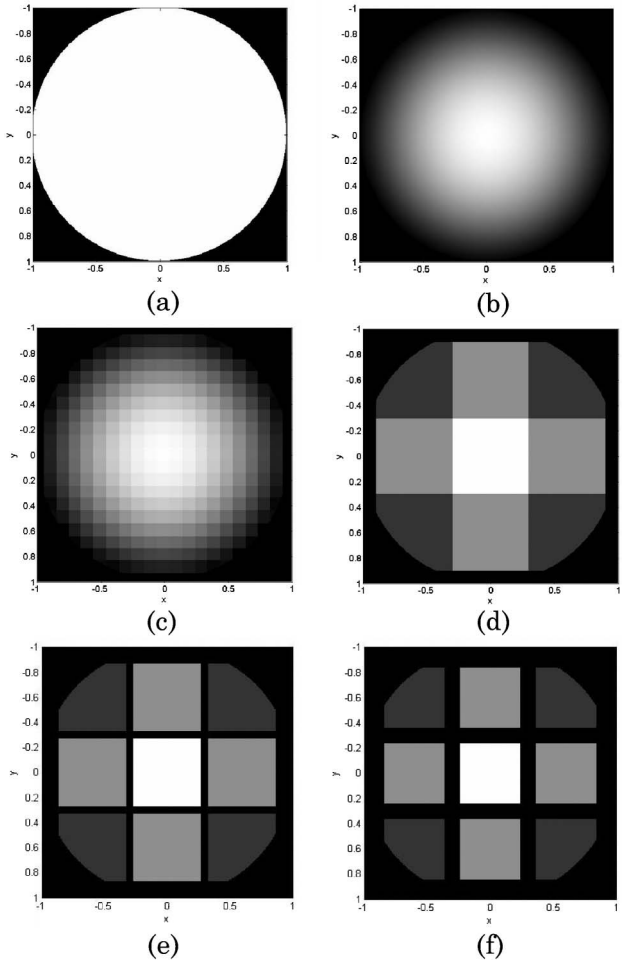

Fig. 3. Total aperture functions on the aperture stop, which are generated by the DMD in the conditions of (a) clear aperture, (b) $K = 0$, (c) $K = 0.05$, (d) $K = 0.3$, with fill factor 100%, (e) $K = 0.3$ with fill factor 90%, and (f) $K = 0.3$ with fill factor 80%.

4. Optical Transfer Function of Shaped Pupil

The OTF is derived from the autocorrelation of the pupil function by using the Hopkins canonical coordinate [11] and is given by

$$\tau(s) = \frac{g(s,0)}{g(0,0)} = \frac{\int_{-\infty}^{\infty}\int_{-\infty}^{\infty} f(x+s/2,y)f^*(x-s/2,y)\mathrm{d}x\mathrm{d}y}{\int_{-\infty}^{\infty}\int_{-\infty}^{\infty} f(x,y)f^*(x,y)\mathrm{d}x\mathrm{d}y}, \quad (7)$$

where $f(x,y)$ is the pupil function shown in Eq. (1), $f^*(x,y)$ is the complex conjugate of $f(x,y)$, and s is defined as the spatial frequency $s \equiv 2F\lambda N$. Here F is the f number of the projection lens system, λ is the wavelength, and N is the number of cycles per unit length in the image plane. The value of F is equal to the effective focal length divided by D, where D is the diameter of the effective aperture stop, and the effective focal length is determined by the optical magnification of the projection lens. The denominator of Eq. (7) is the normalizing factor for making $\tau_0(0) = 1$. The $g(s,0)$ and $g(0,0)$ in the OTF for the pupil function $f(x,y)$ can then be given by

$$g(s,0) = \int_{-[1-(s/2)^2]^{1/2}}^{[1-(s/2)^2]^{1/2}} \int_{-[(1-y^2)^{1/2}-s/2]}^{[(1-y^2)^{1/2}-s/2]} T'\left(x+\frac{s}{2},y\right) \cdot T'\left(x-\frac{s}{2},y\right) \times \exp\left\{i2ksx\left[\omega_{20}+\omega_{40}\left(2x^2+2y^2+\frac{s^2}{2}\right)+\omega_{31}y\right]\right\}\mathrm{d}x\mathrm{d}y, \quad (8)$$

$$g(0,0) = \int_{-1}^{1}\int_{-(1-y^2)^{1/2}}^{(1-y^2)^{1/2}} [T'(x,y)]^2\mathrm{d}x\mathrm{d}y. \quad (9)$$

Equations (8) and (9) can be further modified as

$$g(s,0) = \sum_{q'=-p'}^{p'}\left\{\int_{-[(1-y^2)^{1/2}-s/2]}^{[(1-y^2)^{1/2}-s/2]} T'\left(x+\frac{s}{2},y\right) \cdot T'\left(x-\frac{s}{2},y\right) \times \exp\left\{i2ksx\left[\omega_{20}+\omega_{40}\left(2x^2+2y^2+\frac{s^2}{2}\right)+\omega_{31}y\right]\right\}\mathrm{d}x\right\}\Delta y, \quad (10)$$

where $y = \frac{[1-(s/2)^2]^{1/2}}{p'} \times q'$, $\Delta y = \frac{[1-(s/2)^2]^{1/2}}{p'}$, and

$$g(0,0) = \sum_{q=-p}^{p}\left\{\int_{-(1-y^2)^{1/2}}^{(1-y^2)^{1/2}} [T'(x,y)]^2\mathrm{d}x\right\} \cdot \Delta y, \quad (11)$$

where $y = (1/p) \times q$, $\Delta y = (1/p)$.

By replacing the integral in Eqs. (8) and (9) with the y axis for the summation in Eqs. (10) and (11), an initial setting of $p = 100$ is made for the number of intervals used to find the value of $\Delta y = [1-(s/2)^2]^{1/2}/p'$ and $\Delta y = 1/p$ for $g(s,0)$ and $g(0,0)$, respectively. Different numbers of y, from $-[1-(s/2)^2]^{1/2}$ to $[1-(s/2)^2]^{1/2}$, are then used to calculate the OTF.

5. Imaging Performance Evaluation

The OTFs of the different pupil functions are numerically computed using Mathematica software [14] based on Eqs. (1)–(4), (10), and (11). We calculated the OTFs and analyzed the image performances of five different cases for the differently shaped apertures in an aberration-free system and the projection systems with defocused aberration, spherical aberration, and the coma aberration.

A. Case 1: Defocus

We calculated the OTFs of the clear aperture, one conventional annual apodizer, and two specifically shaped pupils with the scale ratios $K = 0.05$ and 0.3, respectively, for defocused systems with the defocus coefficients $\omega_{20} = 0$, λ/π, $3\lambda/\pi$, $5\lambda/\pi$, $10\lambda/\pi$, $15\lambda/\pi$, and $20\lambda/\pi$, as shown in Fig. 4, where we assumed that spherical and coma aberration are free, i.e., $\omega_{40} = \omega_{31} = 0$.

For the large values of ω_{20} from $5\lambda/\pi$ to $20\lambda/\pi$, the spatial frequency corresponding to the first zero becomes smaller. Because, generally, the spatial frequency of the first zero represents the resolution limit of a defocused projection system, we can take the first zero as defining the degree of focus for each case. The larger degree of focus in the larger value of ω_{20} commonly represents the longer depth of focus in a defocused system. The OTF of a clear aperture $T(x,y) = 1$ (i.e., a uniform-shaped aperture), is shown in Fig. 4(a), and was investigated in the literature [3]. The OTF of one annual apodizer $T(x,y) = 1-(x^2+y^2)$, at $(x^2+y^2 \leqq 1)$ and 0 at $(x^2+y^2 > 1)$ with $K = 0$, is shown in Fig. 4(b), and was previously investigated and proven by the use of the theoretical and experimental approaches in the literature [3]. Two former cases are computed again here for comparison. For the large values of ω_{20}, especially those greater than $5\lambda/\pi$, the degree of focus for the shaped pupil with a scale ratio K of less than 0.3, as shown in Fig. 4(c) and 4(d), is significantly larger than that for the clear aperture $T(x,y) = 1$. It is evident that the specifically shaped pupil, which is generated by the DMD with a scale ratio $K = 0.3$ or less, can significantly extend the depth of focus, compared to a clear aperture in the conventional imaging system. We also compared the OTF of the different scale ratios K to the OTF of the conventional annual apodizer $T(x,y) = 1-(x^2+y^2)$. The OTF value of the former increased and came close to the OTF value of the latter when the scale ratio K decreased gradually. In Figs. 4(b) and 4(c), it shows that the OTFs of the specifically shaped pupil with a scale ratio $K = 0.05$ or

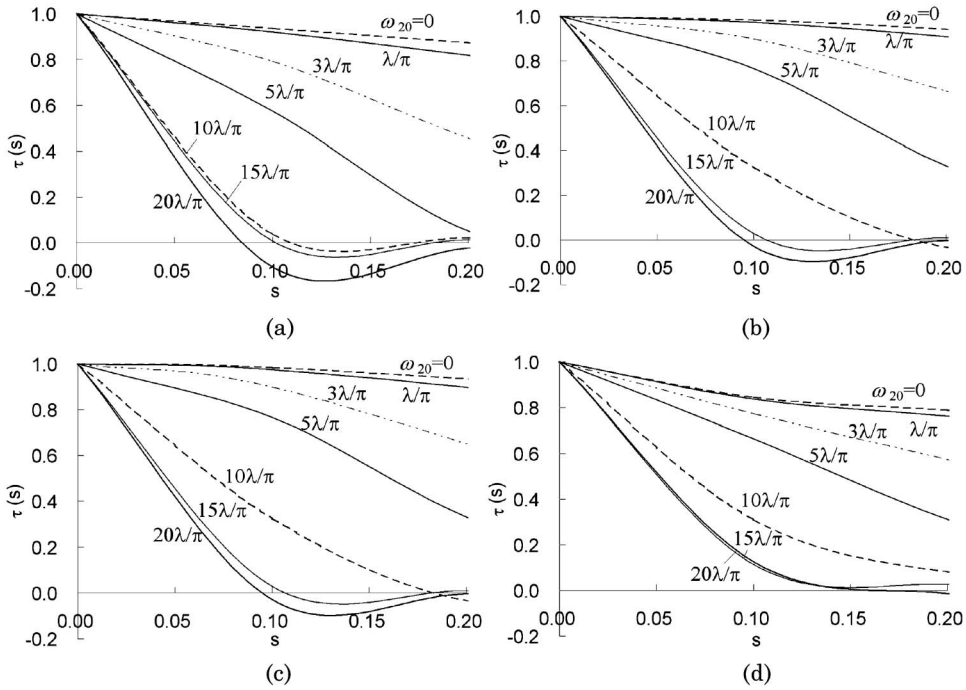

Fig. 4. Optical transfer functions in an aberration-free imaging system and a defocused projection system without spherical aberration $\omega_{40} = 0$ and coma aberration $\omega_{31} = 0$, but with different defocus coefficients $\omega_{20} = 0$, $\omega_{20} = \lambda/\pi$, $\omega_{20} = 3\lambda/\pi$, $\omega_{20} = 5\lambda/\pi$, $\omega_{20} = 10\lambda/\pi$, $\omega_{20} = 15\lambda/\pi$, and $\omega_{20} = 20\lambda/\pi$ for amplitude transmittances of the aperture functions for (a) clear aperture, (b) $K = 0$, (c) $K = 0.05$, and (d) $K = 0.3$.

less can coincide with the OTF of the conventional annular apodizer with continuously shaped aperture. For the case of $K = 0.3$, i.e., the scale ratio K now increases, as shown in Fig. 4(d), the OTF value decreases in the low spatial frequency region, especially for the defocus coefficients ω_{20} less than λ/π. But the OTF value increases in the high spatial frequency region, especially for ω_{20} greater than $10\lambda/\pi$, when $K = 0.3$. It indicates that the degree of focus can increase for the specifically shaped pupil in the defocused projection system when K increases. This is a result of weighting the light intensity from the Airy disk to the rings of the diffraction pattern when designing the specifically shaped pupil in the imaging system for extending the depth of focus [2].

To highlight the capability of our approach, we took a resolution pattern to explore the projection image performance. This pattern is 1951 United States Air Force resolution test chart [15] conforms to MIL-STD-150A standard with resolution 600 dpi× 600 dpi. Referring to Fig. 5, in column (a), one could see the images for the clear aperture, while in columns (b) and (c), the images for the specifically shaped apertures with scale ratios $K = 0.05$ and $K = 0.3$ are shown, respectively. The images were generated by the multiplication of OTF in the Fourier domain using the convolution technique. Furthermore, the images with defocus coefficients of $\omega_{20} = 5\lambda/\pi$, $\omega_{20} = 10\lambda/\pi$, $\omega_{20} = 15\lambda/\pi$, and $\omega_{20} = 20\lambda/\pi$, are shown in rows (1)–(4), respectively. Compared with the images for the specifically shaped apertures, the images of the typical aperture show a clearer loss in contrast at high spatial frequencies with larger ω_{20}. Especially for $\omega_{20} \geq 10\lambda/\pi$, there is a significant enhancement of the image resolution at high spatial frequency by the use of a specifically shaped aperture with $K = 0.3$.

B. Case 2: Spherical Aberration

Here we turn to focus on the clarification of the influence of spherical aberration. The spherical aberration is the essential aberration along the optical axis, i.e., on-axis aberration. We calculated the OTFs of the clear aperture, one conventional annual apodizer, and two specifically shaped pupils with the scale ratios $K = 0.05$ and 0.3, respectively, for the projection systems with the coefficients for spherical aberration $\omega_{40} = 0$, λ/π, $3\lambda/\pi$, $5\lambda/\pi$, $10\lambda/\pi$, $15\lambda/\pi$, and $20\lambda/\pi$, as shown in Fig. 6, if we assumed that defocused and coma aberration are free, i.e., $\omega_{20} = \omega_{31} = 0$. The OTF of a clear aperture $T(x,y) = 1$ (i.e., a uniform-shaped aperture), is shown in Fig. 6(a). The OTF of one annual apodizer $T(x,y) = 1 - (x^2 + y^2)$, at $(x^2 + y^2 \leqq 1)$ and 0 at $(x^2 + y^2 > 1)$ with $K = 0$, is shown in Fig. 6(b). The OTFs for the shaped pupil with a scale ratio K of less than 0.3, as shown in Figs. 6(c) and 6(d), are significantly larger than that for the clear aperture $T(x,y) = 1$ in Fig. 6(a) at all spatial frequency.

It is evident that the specifically shaped pupil, which is generated by DMD with a scale ratio $K = 0.3$ or less, can significantly extend the depth of focus, compared to a clear aperture in the conventional imaging system with spherical aberration. The

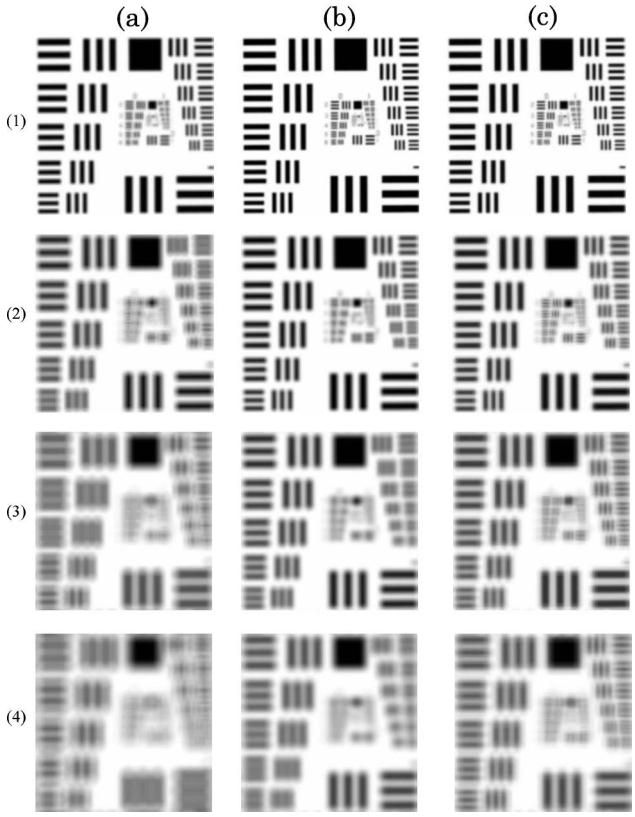

Fig. 5. Computer-simulated images of resolution patterns for (a) a clear aperture and (b) a specifically shaped aperture with the scale ratio $K = 0.05$, and (c) a specifically shaped aperture with the scale ratio $K = 0.3$, obtained with different defocus coefficients: (1) $\omega_{20} = 5\lambda/\pi$, (2) $\omega_{20} = 10\lambda/\pi$, (3) $\omega_{20} = 15\lambda/\pi$ and (4) $\omega_{20} = 20\lambda/\pi$.

OTF of $K = 0.3$ is slightly lower than, but similar to, that of $K = 0.05$ in Figs. 6(c) and 6(d). It indicates that the degree of focus could be similar for the specifically shaped pupil in the projection system with spherical aberration when K varies from 0.05 to 0.3. We also compared the OTF of the different scale ratios K to the OTF of the conventional annual apodizer $T(x,y) = 1 - (x^2 + y^2)$. The OTF value of the former increased and came close to the OTF value of the latter when the scale ratio K decreased gradually. In Figs. 6(b) and 6(c), it shows that the OTFs of the specifically shaped pupil with a scale ratio $K = 0.05$ or less can coincide with the OTF of the conventional annular apodizer with a continuously shaped aperture.

We also took a resolution pattern [15] to explore the projection image performance in the projection system with spherical aberration. Referring to Fig. 7, in column (a), one could see the images for the clear aperture, while in columns (b) and (c), the images for the specifically shaped apertures with scale ratios $K = 0.05$ and $K = 0.3$ are shown, respectively. Furthermore, the images with spherical-aberration coefficients of $\omega_{40} = 5\lambda/\pi$, $\omega_{40} = 10\lambda/\pi$, $\omega_{40} = 15\lambda/\pi$, and $\omega_{40} = 20\lambda/\pi$, are shown in rows (1)–(4), respectively. Spherical aberration could make the image of a bright point source surrounded by a halo of light. The effect of spherical aberration on an extended image is to soften the contrast of the image and to blur its details with symmetrical distribution. Compared with the images for the specifically shaped apertures, the images of the clear aperture show a clearer loss in contrast and a seriously blurred flare at all spatial frequency with larger ω_{40}, even though the three-bar charts for all spatial frequencies is resolved for the clear aperture. Especially for $\omega_{40} \geq 10\lambda/\pi$, there is a significant enhancement of the imaging contrast by the use of a specifically shaped aperture with $K = 0.3$ and 0.05.

C. Case 3: Coma Aberration

In this subsection, we consider the influence of coma and its compensation. Coma is treated as the essential off-axis aberration. We calculated the OTFs of the clear aperture, one conventional annual apodizer, and two specifically shaped pupils with the scale ratios $K = 0.05$ and 0.3, respectively, for the projection systems with the coefficients for coma aberration $\omega_{31} = 0$, λ/π, $3\lambda/\pi$, $5\lambda/\pi$, $10\lambda/\pi$, $15\lambda/\pi$, and $20\lambda/\pi$, as shown in Fig. 8, where we assumed that defocused and spherical aberration are free, i.e., $\omega_{20} = \omega_{40} = 0$. The OTF of a clear aperture $T(x,y) = 1$ is shown in Fig. 8(a). The OTF of one annual apodizer $T(x,y) = 1 - (x^2 + y^2)$, at $(x^2 + y^2 \leqq 1)$ and 0 at $(x^2 + y^2 > 1)$ with $K = 0$, is shown in Fig. 8(b). The OTFs for the shaped pupil with a scale ratio K of less than 0.3, as shown in Fig. 8(c) and 8(d), are significantly larger than that for the clear aperture $T(x,y) = 1$ in Fig. 8(a) at all spatial frequency.

It is evident that the specifically shaped pupil, which is generated by DMD with a scale ratio $K = 0.3$ or less, can significantly extend the depth of focus compared to a clear aperture in the conventional imaging system with coma aberration. The OTF of $K = 0.3$ is slightly lower than, but similar to, that of $K = 0.05$ in Figs. 8(c) and 8(d). It indicates that the degree of focus could be similar for the specifically shaped pupil in the projection system with coma aberration when K varies from 0.05 to 0.3. We also compared the OTF of the different scale ratios K to the OTF of the conventional annual apodizer $T(x,y) = 1 - (x^2 + y^2)$. The OTF value of the former increased and came close to the OTF value of the latter when the scale ratio K decreased gradually. Figures 8(b) and 8(c) show that the OTFs of the specifically shaped pupil with a scale ratio $K = 0.05$ or less can coincide with the OTF of the conventional annular apodizer with a continuously shaped aperture.

We also took a resolution pattern to explore the projection image performance in the projection system with coma aberration. In order to obviously show the effect of coma aberration by the use of a suitable test chart, we utilized a concentric-circles pattern with resolution 96 dpi × 96 dpi [16]. Referring to Fig. 9, in column (a), one can see the images for the clear aperture, while in columns (b) and (c), the

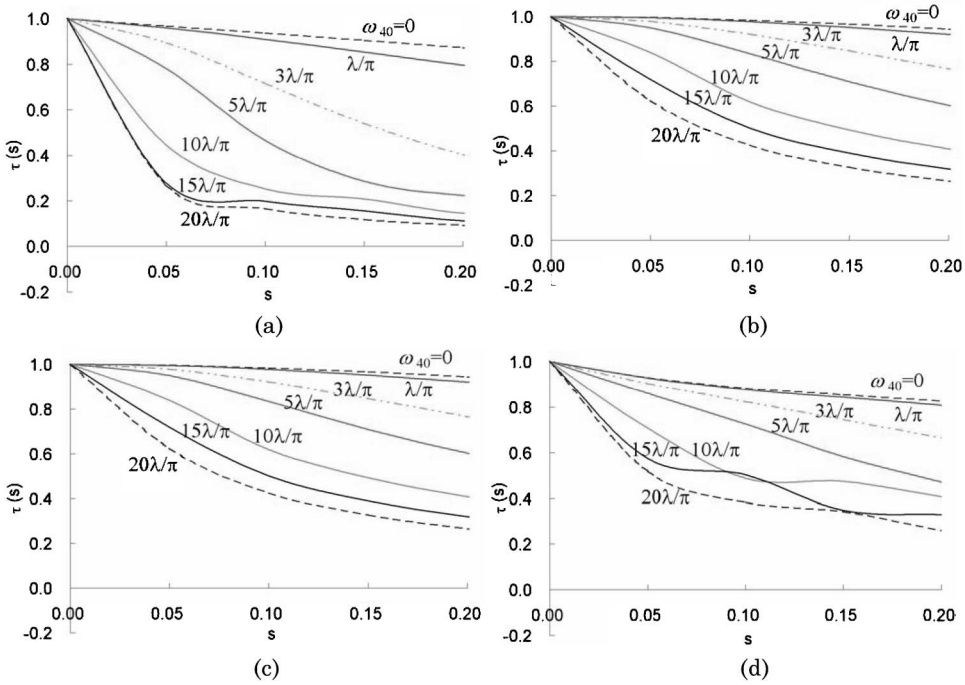

Fig. 6. Optical transfer functions in an aberration-free imaging system and a projection system without defocus aberration $\omega_{20} = 0$ and coma aberration $\omega_{31} = 0$, but with different spherical aberration coefficients $\omega_{40} = 0$, $\omega_{40} = \lambda/\pi$, $\omega_{40} = 3\lambda/\pi$, $\omega_{40} = 5\lambda/\pi$, $\omega_{40} = 10\lambda/\pi$, $\omega_{40} = 15\lambda/\pi$, and $\omega_{40} = 20\lambda/\pi$ for amplitude transmittances of the aperture functions for (a) clear aperture, (b) $K = 0$, (c) $K = 0.05$, and (d) $K = 0.3$.

images for the specifically shaped apertures with scale ratios $K = 0.05$ and $K = 0.3$ are shown, respectively. Furthermore, the images with coma aberration coefficients of $\omega_{31} = 5\lambda/\pi$, $\omega_{31} = 10\lambda/\pi$, $\omega_{31} = 15\lambda/\pi$, and $\omega_{31} = 20\lambda/\pi$, are shown in rows (1)–(4), respectively. Coma aberration could make the image of a point source spread out into a comet-shaped flare with the nonsymmetrical distribution. Compared with the images for the specifically shaped apertures, the images of the clear aperture show a seriously blurred flare at all spatial frequency with larger ω_{31} along the vertical direction. Especially for $\omega_{31} \geq 10\lambda/\pi$, there is a significant enhancement of the imaging resolution by the use of a specifically shaped aperture with $K = 0.3$ and 0.05.

D. Case 4: Combined Aberration (Defocus, Spherical Aberration, and Coma)

Now we can consider the whole influence with all aberrations discussed above. We calculated the OTFs of the clear aperture, one conventional annual apodizer, and two specifically shaped pupils with the scale ratios $K = 0.05$ and 0.3, respectively, for the projection systems with a specific defocus coefficient ω_{20}, and the specific coefficients for spherical aberration ω_{40} and coma aberration ω_{31}. For variable spherical aberration, the best focal plane in the condition of $\omega_{20} = -\omega_{40}$ is supposed [17]. The OTFs for $-\omega_{20} = \omega_{40} = \omega_{31} = 0$, $5\lambda/\pi$, $10\lambda/\pi$, and $20\lambda/\pi$ are shown in Fig. 10, respectively. For the large value of the coefficient especially for $20\lambda/\pi$, the degree of focus for the shaped pupil with a scale ratio K of less than 0.3, as shown in Figs. 10(c) and 10(d), is significantly larger

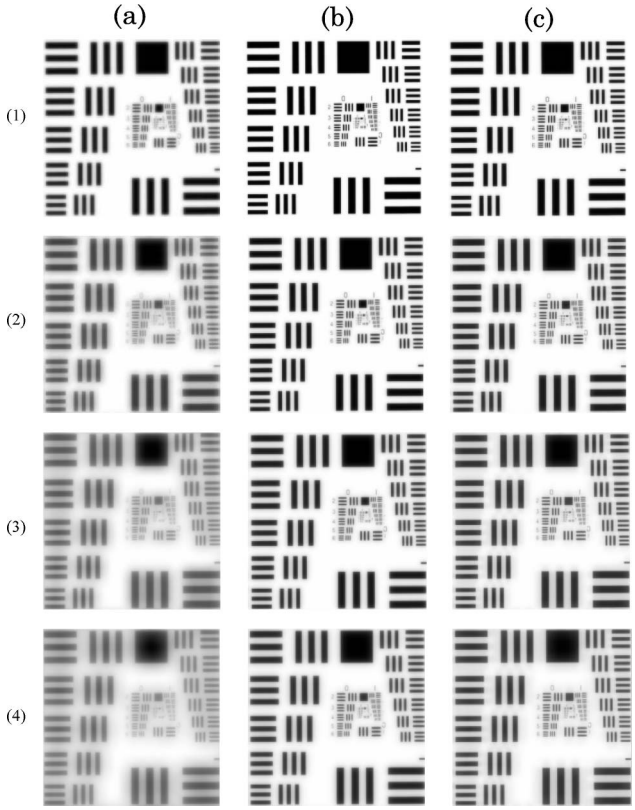

Fig. 7. Computer-simulated images of resolution patterns for (a) a clear aperture, (b) a specifically shaped aperture with the scale ratio $K = 0.05$, and (c) a specifically shaped aperture with the scale ratio $K = 0.3$, obtained with different spherical aberration coefficients: (1) $\omega_{40} = 5\lambda/\pi$, (2) $\omega_{40} = 10\lambda/\pi$, (3) $\omega_{40} = 15\lambda/\pi$, and (4) $\omega_{40} = 20\lambda/\pi$.

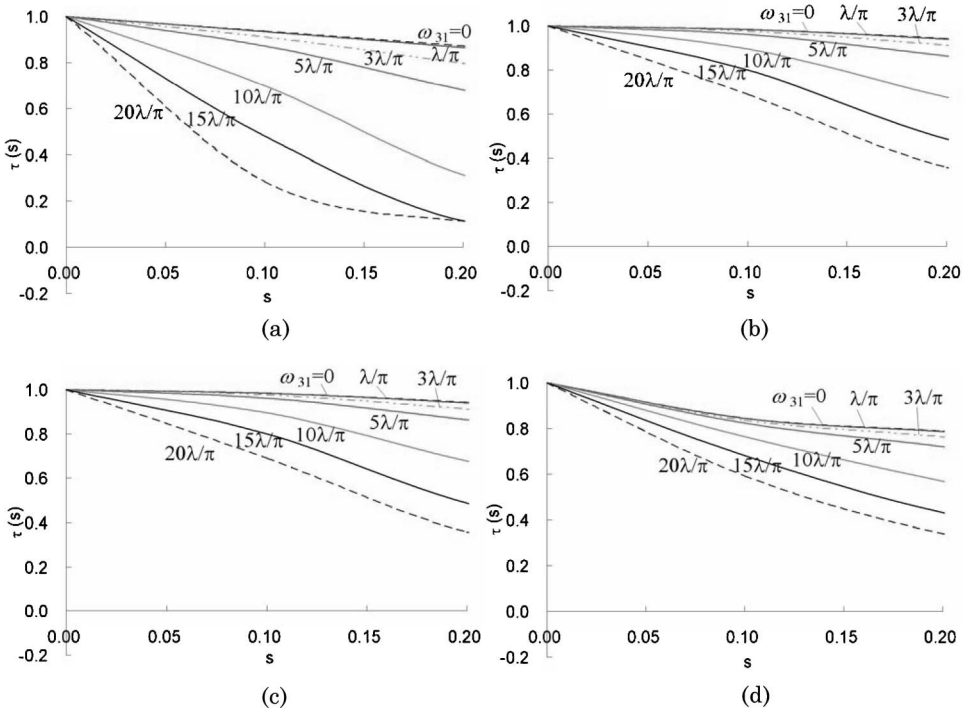

Fig. 8. Optical transfer functions in an aberration-free imaging system and a projection system without defocus aberration $\omega_{20} = 0$ and spherical aberration $\omega_{40} = 0$, but with different coma aberration coefficients $\omega_{31} = 0$, $\omega_{31} = \lambda/\pi$, $\omega_{31} = 3\lambda/\pi$, $\omega_{31} = 5\lambda/\pi$, $\omega_{31} = 10\lambda/\pi$, $\omega_{31} = 15\lambda/\pi$, and $\omega_{31} = 20\lambda/\pi$ for amplitude transmittances of the aperture functions for (a) clear aperture, (b) $K = 0$, (c) $K = 0.05$, and (d) $K = 0.3$.

than that for the clear aperture $T(x,y) = 1$ in Fig. 10(a). It is evident that the specifically shaped pupil, which is generated by DMD with a scale ratio $K = 0.3$ or less can significantly extend the depth of focus compared to a clear aperture in the conventional imaging system. We also compared the OTF of the different scale ratios K to the OTF of the conventional annual apodizer $T(x,y) = 1 - (x^2 + y^2)$. The OTF value of the former increased and came close to the OTF value of the latter when the scale ratio K decreased gradually. Figures 10(b) and 10(c) show that the OTFs of the specifically shaped pupil with a scale ratio $K = 0.05$ or less can coincide with the OTF of the conventional annular apodizer with a continuously shaped aperture.

To highlight the capability of our approach, we took a resolution pattern [15] to explore the projection image performance. Referring to Fig. 11, in column (a), one can see the images for the clear aperture, while in columns (b) and (c), the images for the specifically shaped apertures with scale ratios $K = 0.05$ and $K = 0.3$ are shown, respectively. Furthermore, the images with the aberration coefficients of $-\omega_{20} = \omega_{40} = \omega_{31} = 5\lambda/\pi$, $10\lambda/\pi$, and $20\lambda/\pi$ including defocus, spherical and come aberrations are shown in rows (1)–(3), respectively. Compared with the images for the specifically shaped apertures, the images of typical aperture show a significant loss in contrast at all spatial frequency. Especially for the aberration coefficients $\geq 5\lambda/\pi$, there is a significant enhancement of the image resolution at all spatial

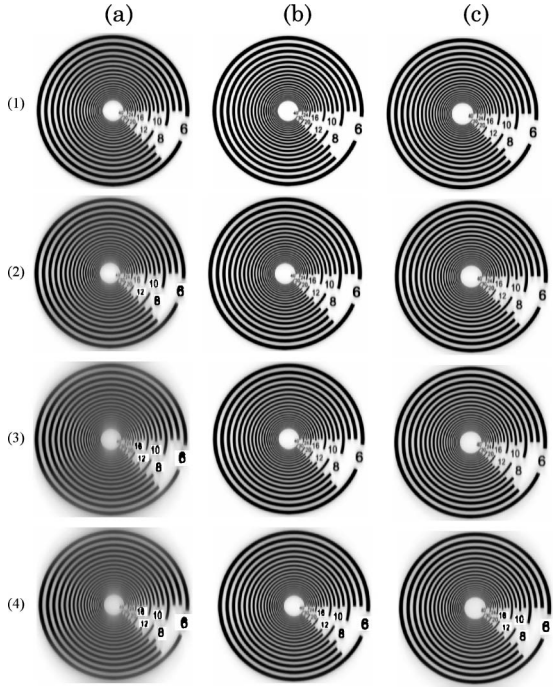

Fig. 9. Computer-simulated images of resolution patterns for (a) a clear aperture, (b) a specifically shaped aperture with the scale ratio $K = 0.05$, and (c) a specifically shaped aperture with the scale ratio $K = 0.3$, obtained with different coma aberration coefficients: (1) $\omega_{31} = 5\lambda/\pi$, (2) $\omega_{31} = 10\lambda/\pi$, (3) $\omega_{31} = 15\lambda/\pi$, and (4) $\omega_{31} = 20\lambda/\pi$.

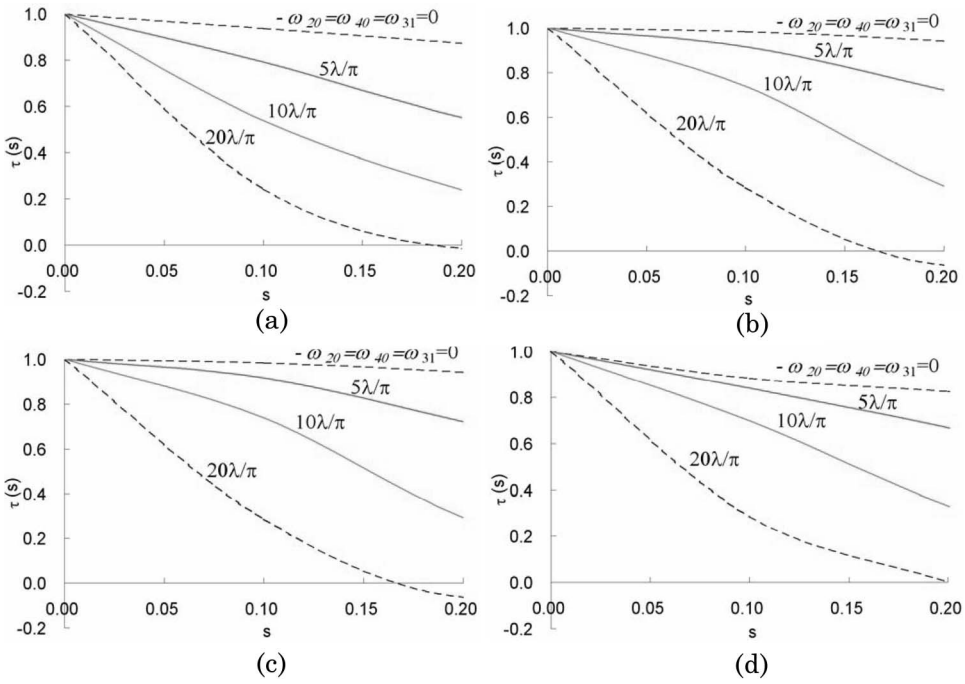

Fig. 10. Optical transfer functions in an aberration-free imaging system and a projection system with different defocus coefficients ω_{20}, different spherical aberration coefficients ω_{41}, and different coma aberration coefficients ω_{31}, when $-\omega_{20} = \omega_{40} = \omega_{31} = 0$, $5\lambda/\pi$, $\omega_{31} = 10\lambda/\pi$, and $\omega_{31} = 20\lambda/\pi$ for amplitude transmittances of the aperture functions for (a) clear aperture, (b) $K = 0$, (c) $K = 0.05$, and (d) $K = 0.3$.

frequency by the use of a specifically shaped aperture with $K = 0.05$ and $K = 0.3$.

Finally, we investigated an example of a real implement for a light value with a typical pixel size equal to 13 μm square in a projection system with $F/\# = 2.0$ and the dominant wavelength $\lambda = 550$ nm. $N = 1/2(13 \times 10^{-6})$ is the number of cycles per unit length in image plane. In this case, $s \equiv 2F\lambda N = 0.085$ is defined as the spatial frequency. Referring to Figs. 4, 6, 8, and 10, we calculated and summarized the OTF values of the clear aperture and two specifically shaped pupils with the scale ratios $K = 0.05$ and $K = 0.3$, respectively, in the cases of ω_{20}, ω_{40}, $\omega_{31} = 0$, $5\lambda/\pi$, $10\lambda/\pi$, and $20\lambda/\pi$ in the condition of a specifically spatial frequency $s = 0.085$ in Table 1. It indicates that the OTFs of a specifically shaped aperture with $K = 0.05$ and $K = 0.3$ are greater than the OTFs of a clear aperture, especially when the aberration coefficients $\geq 5\lambda/\pi$. Hence, we can conclude

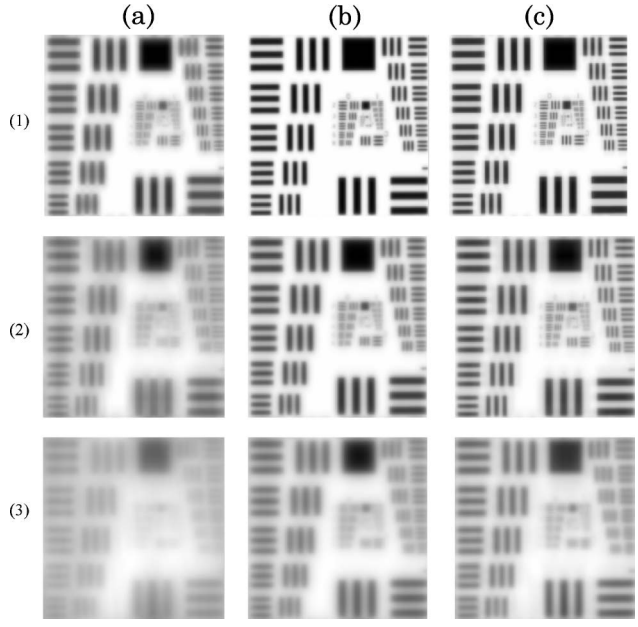

Fig. 11. Computer-simulated images of resolution patterns for (a) a clear aperture, (b) a specifically shaped aperture with the scale ratio $K = 0.05$, and (c) a specifically shaped aperture with the scale ratio $K = 0.3$, obtained with different defocus coefficients ω_{20}, different spherical aberration coefficients ω_{41}, and different coma aberration coefficients ω_{31}, when $-\omega_{20} = \omega_{40} = \omega_{31} =$ (1) $5\lambda/\pi$, (2) $10\lambda/\pi$, and (3) $20\lambda/\pi$.

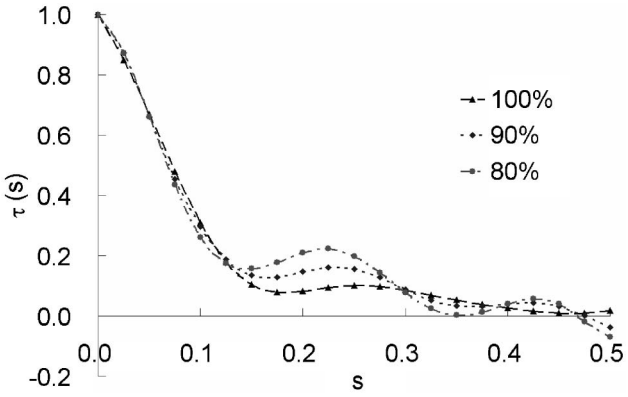

Fig. 12. Optical transfer functions in a defocused system with amplitude transmittances of the aperture functions for $a/D = 0.3$ and the defocus coefficient $\omega_{20} = 10\lambda/\pi$ for different fill factors: 100%, 90%, and 80%.

Table 1. Optical Transfer Function Values of Clear Aperture and Two Specifically Shaped Pupils

Aberration Coefficient	0			$5\lambda/\pi$			$10\lambda/\pi$			$20\lambda/\pi$		
Pupil Shape	Clear Aperture	$K = 0.05$	$K = 0.3$	Clear Aperture	$K = 0.05$	$K = 0.3$	Clear Aperture	$K = 0.05$	$K = 0.3$	Clear Aperture	$K = 0.05$	$K = 0.3$
Defocus (ω_{20})	0.95	0.98	0.86	0.64	0.81	0.71	0.13	0.41	0.38	0.00	0.07	0.22
Spherical (ω_{40})	0.95	0.98	0.90	0.55	0.87	0.77	0.28	0.68	0.54	0.17	0.47	0.41
Coma (ω_{31})	0.95	0.98	0.86	0.90	0.97	0.84	0.75	0.92	0.80	0.36	0.74	0.65
Combination[a]	0.95	0.98	0.90	0.83	0.94	0.87	0.60	0.78	0.75	0.33	0.37	0.37

[a]Combination consists of defocused aberration ($\omega_{20} = -\omega_{40}$), spherical aberration (ω_{40}), and coma aberration (ω_{31}).

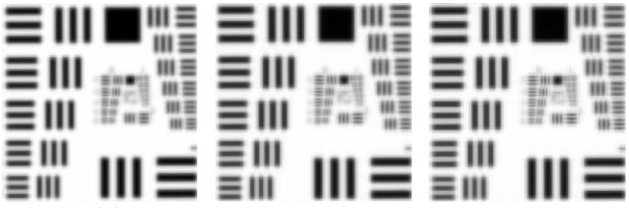

Fig. 13. Computer-simulated images of resolution patterns for a specific shaped aperture with the scale ratio $a/D = 0.3$ and different fill factors (a) 100%, (b) 90%, and (c) 80% in a defocus system with the defocus coefficient $\omega_{20} = 10\lambda/\pi$.

that the projection quality will be enhanced as the specifically shaped aperture is used, especially for the imaging system with large aberration coefficients, including defocus, spherical, and come aberrations. In other words, as for a real implementation of an illumination modulator with DMD, the specifically shaped pupil can improve the projection quality compared to a clear aperture in the conventional projector system.

E. Case 5: Influence of Fill Factor

In order to evaluate the relationship between image performance and the size of the individual square aperture on the normalized pupil, we computed the OTFs of the other types of pupil functions based on Eqs. (1), (5), (10), and (11) in a defocused system with the defocus coefficient $\omega_{20} = 10\lambda/\pi$ and the amplitude transmittances of the aperture functions for $a/D = 0.3$ with different fill factors 100%, 90%, and 80% in Fig. 12.

The degree of focus (i.e., the resolution limit) reduces, but the OTF (i.e., image quality) increases at the specific spatial frequency when the fill factor decreases from 100% to 80%. Furthermore, we took a resolution pattern [15] to simulate the imaging performances for these specifically shaped apertures with the scale ratio $a/D = 0.3$, and different fill factors ranged from 100% to 80% in a defocus system with the defocus coefficient $\omega_{20} = 10\lambda/\pi$, as shown in Fig. 13. Compared with the computer-simulated images in the figure, it shows that the image quality could not be significantly influenced when the fill factor (i.e., aperture ratio) of the spatially shaped pupil varied from 100% to 80%.

6. Conclusions

We have provided a new approach for improving the image quality for a projector system with a specific illuminator modulator. The approach could be also applied to imaging system, as partially explored in Ref. [9]. The semianalytical results using the OTF indicated that the depth of focus can be extended with specifically shaped illumination, which is generated by a digital micromirror device on the aperture stop in the projection system with a specific defocus coefficient and the specific coefficients for spherical aberration and coma aberration.

In summary: (i) the limiting resolution of a defocused projection system with a specific defocus coefficient can be improved by its corresponding binary shaped pupil. It has been shown that a shaped pupil with a scale ratio K equal to 0.05 is more helpful for extending the depth of focus at low spatial frequency, while a shaped pupil with a scale ratio K equal to 0.3 is more useful for extending the depth of focus at high spatial frequency. (ii) In a projection system with the coefficient for spherical aberration or coma aberration, respectively, the OTF for the shaped pupil with a scale ratio K of less than 0.3 is significantly larger than that for the clear aperture at all spatial frequencies. Especially for $\omega_{40} \geq 10\lambda/\pi$ and $\omega_{31} \geq 10\lambda/\pi$, there is a significant enhancement of the imaging contrast by the use of a specifically shaped aperture with $K = 0.3$ and 0.05, according to the computer-simulated image. (iii) The OTFs of a specifically shaped aperture with $K = 0.05$ and $K = 0.3$ are greater than the OTFs of a clear aperture, especially when the aberration coefficients are $\geq 5\lambda/\pi$. It is evident that the projection quality will be enhanced as the specifically shaped aperture is used, especially for the imaging system with large aberration coefficients, including defocus and spherical and come aberrations. (iv) The image quality could not be significantly influenced as the fill factor (i.e., aperture ratio) of the spatially shaped pupil varied from 100% to 80%.

Overall, the proposed approach of a shaped pupil from an illumination modulator is a dynamically programmable method to achieve aberration compensation for projector applications. This method provides a connection between nonimaging and imaging systems for enhancing the projection quality. Regarding that the pupil aberration is considered in the illumination system, this influence may be incorporated with the corresponding spherical aberration and even off-axis coma with different levels of coefficients. Hence, practically, the pupil aberration could be included partially and further explored once the spherical aberration and coma are included. It is worth noting that this proposed model can rapidly and field-sequentially generate a specifically shaped pupil with 10 gray levels within the very short image processing time of 0.22 ms in the case of $K = 0.05$. Different spatial frequencies represent different imaging information from the light value in a projector system. High spatial frequencies represent sharp spatial changes in the image, such as edges, and generally correspond to local information and fine detail, while the portion of low spatial frequencies represent global information about the shape, such as general proportion and orientation. On the other hand, this shape-programmable pupil with specific scale ratios K, which are generated by the illumination modulator in a projector, can dynamically provide very high projection image quality when many varied scenes with global information (i.e., low spatial frequencies) and with local information (i.e., high spatial frequencies) sequentially perform on the screen.

This work was supported in part by the National Science Council of Taiwan (NSCT) under project 93-2215-E-009-057 and in part by the Ministry of

Education and the Academic Top University program at the National Chiao Tung University, Taiwan.

References

1. E. H. Stupp and M. S. Brennesholtz, *Projection Display* (Wiley, 1999).
2. J. W. Goodman, *Introduction to Fourier Optics*, 3rd ed. (Roberts, 2005).
3. M. Mino and Y. Okano, "Improvement in the OTF of a defocused optical system through the use of shaded apertures," Appl. Opt. **10**, 2219–2225 (1971).
4. J. Ojeda-Castaneda, P. Andrea, and A. Diaz, "Annular apodizers for low sensitivity to defocus and to spherical aberration," Opt. Lett. **11**, 487–489 (1986).
5. C. S. Chung and H. H. Hopkins, "Influence of nonuniform amplitude on the optical transfer function," Appl. Opt. **28**, 1244–1250 (1989).
6. J. A. Davis, J. C. Escalera, J. Campos, A. Marquez, and M. J. Yzuel, "Programmable axial apodizing and hyperresolving amplitude filters with a liquid-crystal spatial light modulator," Opt. Lett. **24**, 628–630 (1999).
7. A. Marquez, C. Iemmi, J. Campos, J. C. Escalera, and M. J. Yzuel, "Programmable apodizer to compensate chromatic aberration effects using a liquid-crystal spatial light modulator," Opt. Express **13**, 716–730 (2005).
8. J. van der Gracht and W. T. Rhodes, "Source sampling for incoherent imaging and spatial filtering," J. Opt. Soc. Am. A **6**, 1165–1167 (1989).
9. C. M. Cheng and J. L. Chern, "Programmable apodizer in incoherent imaging systems using a digital micromirror device," Opt. Eng. **49**, 023201 (2010).
10. D. Dudley, W. Duncan, and J. Slaughter, "Emerging digital micromirror device (DMD) application," Proc. SPIE **4985**, 14–15 (2003).
11. H. H. Hopkins, "The frequency response of a defocused optical system," Proc. R. Soc. London Ser. A **231**, 91–103 (1955).
12. C. M. Cheng and J.-L. Chern, "Design of a dual-*F*-number illumination system and its application to projection display with DMD™," J. Soc. Inf. Display **14**, 819–827 (2006).
13. Y. Kwak and L. MacDonald, "Characterisation of a desktop LCD projector," Displays **21**, 179–194 (2000).
14. Mathematica version 4, Wolfram Research, Incorporated, 100 Trade Center Drive, Champaign, Illinois 61820-7237, USA.
15. See http://en.wikipedia.org/wiki/1951_USAF_resolution_test_chart.
16. See http://www.eronn.net/camera/test-chart.
17. V. N. Mahajan, *Optical Imaging and Aberrations: Part II. Wave Diffraction Optics* (SPIE, 2001).